MJSAT

Malaysian Journal of Science and Advanced Technology

journal homepage: https://mjsat.com.my/

Geoengineering Site Exploration for Building, Bridge, Landfill, Pavement, Embankment Construction, and Excavation (Road Cut/Open Pit Mines): Case Study from Southwestern Nigeria

Abayomi Solomon Daramola*[1], Olumuyiwa Olusola Falowo[2], William Kunle Olabisi[1], and Oluwatobi Emmanuel Ajiboye[1]

[1]*Dept. of Civil Engineering Technology, Rufus Giwa Polytechnic Owo, Ondo State, Nigeria.*
[2]*Dept. of Applied Geology, Federal University of Technology Akure, Ondo State, Nigeria.*

KEYWORDS

Schistose quartzite
Groundwater measurement
Geophysical
CPT
Material behaviour index

ARTICLE HISTORY

Received 1 February 2026
Received in revised form 31 May 2026
Accepted 14 June 2026
Available online 28 June 2026

ABSTRACT

T Engineering site exploration of RUGIPO was conducted using integrated methods involving in situ CPT testing, geophysical, geotechnical laboratory studies, geochemical analysis, groundwater measurement and quality analysis, and geological mapping. This was done to assess the geomaterial across the study area for civil engineering construction. The result revealed schistose quartzite and quartzite as the main rocks in the area, capable of providing (compressive) strength of 150 to over 350MPa, and 20 – 60 MPa, respectively. The abundance of SiO2 in the soil mineral content (52.4 %) implies a good engineering tendency that can translate to high CBR, shear strength, and PI, and low compressibility/swelling potential. The soils across the area are dominated by sand - silt mixture, with average CBR (> 10%), cohesion (23.2 kN/m^2), friction angle (29.1°), PI (< 20 %), allowable bearing capacity (172.6 kN/m^2), modulus of elasticity (18715 kN/m^2), soil behaviour index (2.40), and elastic settlement (34.19 mm for 250 kN load). Thus, the soil is expected to have good applications in basement or foundation, reinforced cement concrete structures (including slabs, lintels, and columns), bridge, pavement, metallic grounding systems/utilities, and embankment. However, the soils fail in some major properties for landfill/liners application in terms of PI, permeability, and porosity. The groundwater level is higher than 8 m across the study area; hence, it cannot threaten the basement/foundation structure. The quality of the water is within the recommended threshold for all the parameters tested for, including T°, SG, pH, TDS, EC, salinity, sulfate, and EC, for concrete cement interaction.

1. INTRODUCTION

The significance of site exploration for any civil engineering construction cannot be overemphasized [1], [2], [3] because it serves as the foundation framework on which the durability and safety of the structures would rest on [4], [5], as it would revealed pertinent geological data on settlement, bearing pressure, and hazards that would be unfavorable to the construction [6], [7], [8], such as volcanic activity, flooding, rockfall or slide, earthquake, underground cavity, buried mines, sinkholes, landslides, etc. In addition, it furnishes information on the potential reaction of the site's material with concrete and other engineering materials [9], [10], [11]. Geohazard influences the lithology, compositional attributes, and strength parameters (cohesion and angle of friction) of the material on site, as a result of alteration to their shape, texture (fabric/structure), and mineralogy [12], [13]. As a result, their influence determines the geomechanical behavior of the material under structural loading [14], [15]. As a result, the magnitude of soil/rock damage caused by these geohazards, which manifest as low bearing pressure and differential settlement, cannot be overstated in the construction sector [4], [5], [6], [11]. Even while many engineers typically blame

*Corresponding author:
E-mail address: Abayomi Solomon Daramola < yomidams02@gmail.com >.
https://doi.org/10.56532/mjsat.v6i2.705
2785-8901/

failures on design or building processes, or construction materials, they rarely beam their "torch light" on geological geohazards surrounding the site. This is another reason why many engineers have been unable to comprehend this preventable hazard. Many irritating reports of structural breakdown are broadcast on many communication devices from many geopolitical zones around the country, with no improvement or significant standardized policy on engineering site assessment before the construction phase [10], [16], [17], [18], [19], [20], [21]. Hence, this serious omission or commission must be given serious investigation or attention it deserves. The case is not different in Ondo State, Nigeria, as many civil engineering structures are done without thorough pre-construction investigation. Many campus roads, especially in Rufus Giwa Polytechnic Owo (RUGIPO) in Ondo State, Nigeria, constructed barely a few years ago had failed, likewise other structures. The reason for such failures is not far-fetched. In places where subsoil exploration was carried out, assumption/extrapolation of parameters was usually adopted.

Engineering site exploration can be done directly in situ or indirectly using non-destructive geophysical approaches [22]. Although the geophysical is relatively quick to use, it cannot replace traditional boring, drilling, SPT, CPT, or DCP. It is possible to measure the in-situ properties and structural qualities of earth materials using geotechnical and geophysical techniques. Since the use of such techniques has shown cost savings through less design uncertainty and decreased investigation costs. Geophysics can be used for exploration in the building industry to provide helpful data for the early identification of potentially hazardous subsurface conditions [23], [24], [25], [26], [27]. Essentially, undetected near-surface structures, including holes and/or inhomogeneity in the foundation geomaterials, are the main causes of risks in the civil engineering fields. Geophysical techniques have been used not only for engineering site research, but also for gallery stability, tunneling, foundations, excavation operations, embankment building, railway, highway, and other applications [23], [24], [25], [26], [27]. Geophysical techniques are coupled with remote sensing, geochemical, hydrogeological, and laboratory measurements to provide the best results. In light of this, RUGIPO requires the development of a complete model of predicted soil qualities under various loading scenarios for various civil engineering constructions. This would facilitate and complement government efforts in curbing the "ugly development of structural failure" in the State and the country at large. The soil investigation and test report would also be of help to all these professionals involved in the construction of structures. The study would generate necessary baseline information useful for planning and for developing an appropriate environmental management programme in order to moderate the probable harmful effects of human activity for thorough environmental sustainability [25], [28].

Increasing the scope of the site investigation significantly reduces the risk of foundation failure, potentially saving clients and consultants large sums of money [19], [21]. It would help in imagery any potential hazard (natural and man-made) that could be inimical to the foundation of any civil engineering structure in the proposed research environment. It would serve as an indispensable tool and information for civil engineers that geophysical and geotechnical surveys are essential for preconstruction/design activities [3], [10], [25], [28]. The primary goal of this research is to identify the subsoil/rock's ability to support civil engineering structures and utilities such as buildings, roads, bridges, communication masts, and to predict appropriate/expected bearing capacity and settlement under various loadings. The objectives are to determine the geotechnical and engineering parameters of the proposed site; to determine the depth to competent bedrock in the site; to conduct geological and surface reconnaissance studies of the area; to delineate the subsurface layers underlying and determine their geoelectric characteristics; to determine the overburden thickness (depth to bedrock); and to investigate the structural features of the bedrock such as faults, fractures, joints, lithological boundaries in the institution. The criteria for choosing the research environment was because there had not been any comprehensive geological/geophysical and geotechnical investigation carried out in the environment before, and also recently, constructions on-going in the school premises (even as the school is trying to relocate to the Pre-ND village) necessitated this research. Therefore, the study would provide database information on the engineering suitability of the area to host different kinds of structures. This would invariably reduce uncertainties associated with the design and planning of structures with unknown soil properties.

2. Description of Study Area

RUGIPO is located at northern senatorial district of Ondo State, Nigeria (figure 1). It is located within the tropical rainforest of Nigeria. The annual temperature ranges from 24 to 28°C, and the mean annual rainfall is over 1500mm [29]. The yearly rainfall and other advantageous climatic and geologic influences guarantee sufficient groundwater recharge in the area. The area is underlain by the migmatite-gneiss complex, with granite, gneiss, quartzite, and quartz schist being the rocks in the institution. The gneiss occurs as biotite gneiss and the banded gneiss [30]. The Schist, which is also a metamorphic rock composed mainly of quartz, formed by the action of heat and pressure on sandstone; the quartzite schist/schistose quartzite is a rock that splits into layers whose minerals have aligned themselves in one direction [9]. However, within the main campus, schistose quartzite and quartzite are the main geological/rock units (figure 2).

The topography of the study area (figure 3) is slightly undulating with rounded low hills (found at low rise area and sports complex in the central and eastern zones), occasional, often elongated ridges indicating the characteristic residue setting of a typical basement terrain, with an average height ranging between 20 and 50 m above sea level. The superficial deposit within the basement complex terrain varies in thickness from 2 m to more than 50 m and is mostly clayey loamy topsoil, clayey sand, and sandy clay soil, which can be sandwiched by reddish brown lateritic hardpan (less than 3 m) soil in many places. The drainage map (figure 3) showed the streams in the study area, which are generally disjointed. These streams are limited in length and aerial extent, as the majority are found within the relatively lower elevation regions. These disjointed streams or disjointed drainage patterns would has a detrimental impact on the long-term stability of the groundwater table, generally leading to permanent declines in water levels, reduced aquifer recharge, and increased susceptibility to drought.

3. Material and Methods

The study methods included field and laboratory studies. The field study comprised geological mapping, geophysical, geochemical, geotechnical cone penetration, and laboratory analysis. The geological mapping was carried out with the use of a compass clinometer, hand lens, sledgehammer, camera, and base map (topographical and administrative maps). The laboratory involved analysis of samples for elemental/mineralogical composition and index properties. However, at the beginning of the study, a thorough reconnaissance study was conducted to obtain and confirm additional information from the study area. This includes information on geology/depositional history, topography, vegetation, etc. Also, important information such as land use before the field survey. Preliminary exploration depths were estimated from data obtained during field reconnaissance, existing data, and local experience. Also, areas of sampling were pegged, numbered, and georeferenced consecutively using a global positioning system (GARMIN'S GPS 12 - Channel model). Thirty-three (33) disturbed soil samples were collected from thirty-three different locations and labelled appropriately. The collected samples were analyzed at the engineering geology (for geotechnical analysis according to the BS 1377 [31] procedures) and geochemistry laboratory (for atomic absorption spectrometry) of the Applied Geology Department, Federal University of Technology, Akure, Ondo State, Nigeria. The soil samples were taken based on geology and geomorphology within dug trenches/boring pits at the institution. Each boring/test pit was given a distinctive ID number for easy reference. The ground level altitude and actual location were correctly determined at each sampling location. The collected samples were subjected to grain size analysis, specific gravity determination, natural moisture content test, consistency limit test, compaction test, California bearing ratio, triaxial test, and undrained compressive test. From the results of the laboratory analysis, the bearing capacity was determined. At the points where the samples were taken, the cone penetrometer test/standard penetration test was carried out using 10 tons capacity Dutch-cone penetrometer. The procedure of ASTM D5778-07 [32] was strictly followed when conducting the test.

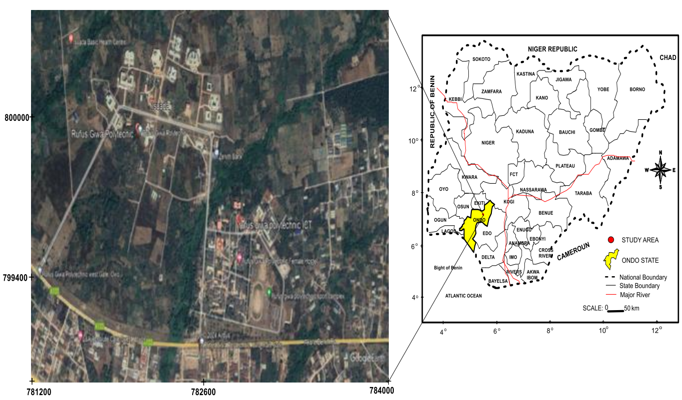

Fig. 1. Location map of the study area

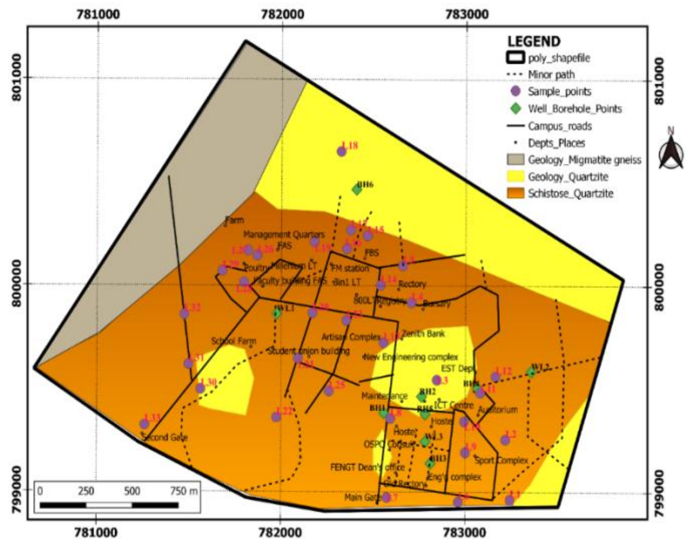

Fig. 2. Geological map of the study area, modified after Geological Survey [33], also showing the sampling points for the well/borehole points, geochemical and geotechnical data locations

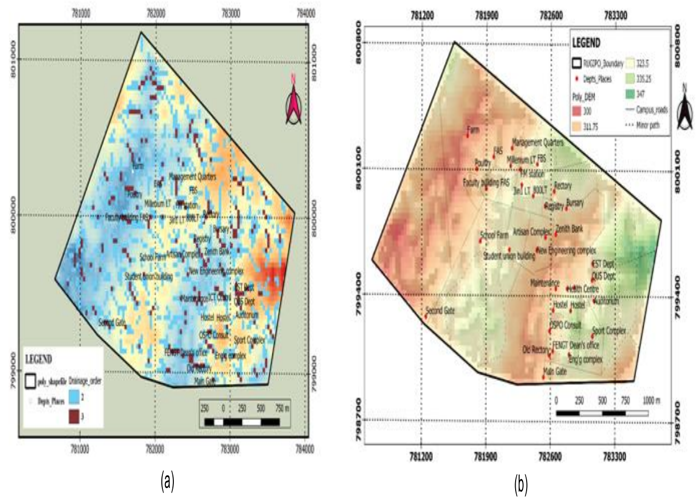

Fig. 3. Map showing (a) the drainage pattern of major streams and (b) the Digital Elevation Model of the study area, with the eastern and central zones showing relatively high relief

The hydrogeological measurement includes the determination of the hydraulic head of wells/boreholes, measurement of static water levels, and water columns in the existing wells and boreholes. Nine well/borehole water samples were taken and measured for physical parameters that have a direct influence on concrete. The parameters measured were total dissolved solids (TDS), electrical conductivity (EC), temperature (T°), salinity, pH, salt (sulfate) concentration, and specific gravity (SG). The parameters were measured using hand held multi-parameter water tester (EC/TDS/SALTS/SALINITY/S.G/ORP/Temperature-066).

The very low frequency electromagnetic field utilizing the ABEM–WADI EM-VLF meter was taken at 1 m spacing. The recordings of both real and quadrature modules were taken. The real component was processed, as they are more linear features. The KHFFILT" software version 1.0 was used for 2-D modeling of the filtered real component for quantitative interpretation. The electrical resistivity utilized VES with Schlumberger array/configuration with half current maximum spacing of 65 m along the traverses, established for the study, with sounding stations marked and pegged at about 20 m spacing. Eighty (80) sounding points were occupied using an Omega resistivity meter. The apparent resistivity data at the station points were plotted against electrode spacing on bilogarithmic graph sheets. The resulting curves emanating from the graphs were examined visually for the nature of the subsurface geological units. Thereafter, the curves undergo partial curve matching for the quantitative interpretation and geoelectric/geological sectioning.

The ground magnetic investigation used a GSM-8 Proton Precision Magnetometer, which is capable of producing an absolute and relative high resolution of the field and displaying measurements in a digital readout. At the beginning of the survey, the base station was situated about 500 m away, where magnetic data and time were initially recorded. Subsequently, the traverse was now occupied, with readings taken at regular station intervals of 1 m. After taking magnetic readings along the traverse, the final base station magnetic reading and time for the traverse were recorded, and the drift/drift constant was determined. The drift correction was performed on the magnetic reading. The processing of the magnetic data includes removing all sources of magnetic deviation/variation from observations that are not magnetic effects of the subsurface. The magnetic data acquired are presented as plots of relative magnetic reading against station position. The interpretation technique adopted is qualitative interpretation, which involves visual examination of profiles and maps to obtain information about the target, such as location, geologic dip direction, and nature of the target.

For the analysis of the foundations concerning bearing capacity, settlement, and other soil parameters determination [33], [34], [35], [36], [37], [38], the CPT was utilized at exactly thirty-three (33) points where samples were collected. The test was conducted in line or agreement with ASTM D5778-07. The obtained results included the friction resistance (qr), end-bearing/cone resistance (qc), and friction ratio (FR), which is computed by dividing qs by qc, were plotted against depth using Grapher software. The CPT data were classified according to Robertson's non-normalized SBT chart [39], which is based on the dimensionless qc and FR. The chart is zoned into nine (9) different zones matching different soil behaviour types (Table 1). The CPT qc values was normalization to the standard overburden pressure of 100 KN/m^2 (Table 2), using the relation in equation 1. The addition of normalized cone resistance and sleeve friction was used in determining other parameters such as cohesion, angle of friction, N-value, and unit weight [40], [41].

$$q_{cn} = C_n q_c \tag{1}$$

C_n = correction value or factor
q_{cn} = normalized q_c due to overburden pressure
From the result of the CPT, soil cohesion (using equations 2 – 4), friction angle (equations 6 and 7), and unit weight (equation 8) were obtained, in assessing the engineering bearing competence of the soil at refusal depth, using the following equations, respectively.

$$c = 0.02 q_c \tag{2}$$

c = cohesion; q_c = value of cone resistance

$$c = -2.2049 + 6.484N; \; 2 \leq N \leq 30 \tag{3}$$

$$c = -16.5 + 2.15N; \; 10 \leq N \leq 30 \tag{4}$$

Friction angle, ø', was estimated by using the following equation [42], which is applicable for SBTn zones 5, 6, 7, and 8, in equation 5. The unit weight was obtained using equation 6.

$$\emptyset' = 17.80 + 11 \log Q_t \tag{5}$$

$$\frac{\gamma}{\gamma_w} = 0.27[log F_R] + 0.36[log \frac{q_c}{\rho_a}] + 1.236 \tag{6}$$

γ_w is the unit weight of water (9.81kN/m^3), ρ_a is atmospheric pressure (0.1MPa), q_c in MPa, γ is the volume weight of soil (kN/m^3), F_R is the resistance ratio (%).The CPT material index (I_c) can be used to identify soil type and its corresponding characteristic value (Table 3), for estimating footing load-displacement response [43]. The I_c was obtained using equation 7.

$$I_c = \sqrt{(3.47 - \log q_{tn})^2 + (\log F_r + 1.22)^2} \tag{7}$$

Table 1. SBT zones [39]

Zone	Soil Behaviour Type (SBT)
1	Sensitive fine-grained
2	Clays-organic
3	Clays: clay to silty clay
4	Silt mixtures: clayey silt and silty clay
5	Sand mixtures: silty sand to sandy silt
6	Sands: clean sands to silty sands
7	Dense sand to gravelly sand
8	Stiff sand to clayey sand (over-consolidated)
9	Stiff fine-grained (over-consolidated)

Table 2. Normalization values for cone resistance data with respect to overburden pressure [39]

ρ_o (kN/m^2)	c_n	ρ_o (kN/m^2)	c_n	ρ_o (kN/m^2)	c_n	ρ_o (kN/m^2)	c_n
20	2.8	120	0.90	220	0.59	320	0.48
40	1.76	140	0.81	240	0.56	340	0.47
50	1.58	150	0.77	250	0.54	350	0.46
60	1.40	160	0.73	260	0.53	360	0.46
80	1.18	180	0.68	280	0.52	380	0.45
100	1.0	200	0.63	300	0.51	400	0.45

The elastic settlement [38] was derived using equation 8 under a loading of 250kN and a footing width of 2 m.

$$s = \frac{qBI\,(1-v)}{E_S} \tag{8}$$

where s = settlement, q = applied footing stress, B = footing width, v = Poisson's ratio, Es = soil modulus, and I = displacement influence factor from elasticity theory. The average relationship between soil permeability (k) and SBT Ic, shown in Table 4, can be represented by equations 9 and 10:

When

$$1.0 < I_c < 3.27 \quad k = 10^{(0.952-3.04I_c)} \text{ m/s} \tag{9}$$

$$3.27 < I_c < 4.0 \quad k = 10^{(0.952-3.04I_c)} \text{ m/s} \tag{10}$$

The Young's Modulus (E_s), was determined using equation 11 [41], while the ultimate bearing capacity was determined using equations 12 and 13 [34], [37] for soil derived from schistose quartzite and quartzite, respectively. In this study, 2 m is the width, and D_e was the embedded depth (taken as CPT refusal depth).

$$E_s = 0.015[10^{0.55I_c+1.68}] \tag{11}$$

$$q_{ult} = (\frac{q_c}{33})^{0.9} \tag{12}$$

$$q_{ult} = q_c(B/12)(1+\frac{D_e}{B})C_w \tag{13}$$

The undrained shear strength [42] was calculated using equation 14, as:

$$S_u = \frac{q_t - \sigma_v}{N_{kt}} \tag{14}$$

where N_{kt} is the undrained shear strength constant. Typical values of N_{kt} vary from 10 to 18, with 14 being the default value. The CBR in % was determined by using equation 11 [40].

$$CBR\ (\%) = 0.454q_c \tag{15}$$

Table 3. CPT index, Classification zones, and corresponding soil [35]

Soil Classification	Zone Number	Range of CPT Index (I_c) Values
Organic clay soils	2	$I_c > 3.22$
Clays	3	$2.82 < I_c < 3.22$
Silt Mixtures	4	$2.54 < I_c < 2.82$
Sand Mixtures	5	$1.90 < I_c < 2.54$
Sands	6	$1.25 < I_c < 1.90$
Gravelly Sands	7	

4. RESULTS AND DISCUSSION

4.1 Groundwater flow potential

Tables 5 and 6 present a summary of the hydrogeological measurements from existing wells and boreholes. Although the wells and boreholes are scarce at the institution, the information obtained from them can be a valuable tool in the design process of structures. The depth to water level, total depth of sampled wells, water column, and hydraulic head ranged from 8.1 – 10.5 m, 11.2 – 15.3 m, 1.3 – 4.8, 316.9 – 330.5, respectively. Though the wells are moderately deep, the water column, which demonstrates the volume of water in the well, is minimal. The depths of the sampled boreholes ranged from 20 to 45 m. figure 4 shows the spatial distribution of SWL and HH across the study area. The SWL is higher in the northern part, especially within the quartzite rocks (can be higher than 30 m), than in the schistose quartzite (less than 10 m). The hydraulic head map (figure 4b) showed that the central part have tendency to water impoundment during the wet season, as they are characterized by low hydraulic head (less than 310 m). Therefore, the foundation for building a structure in the central part must be rafted to counteract this hazard [15]. Excessive water around the foundation structure creates a scouring phenomenon around the structure. In addition, the water can reduce the shear strength and bearing capacity of the soil [44]. Raft foundations are highly effective in areas with high hydraulic head (high groundwater table) because they offer a continuous, impermeable slab that "floats" on the soil, reducing the risk of differential settlement and providing a watertight barrier.

Table 4. Estimated soil permeability (k) based on the CPT SBT chart [35]

SBT Zone	SBT	Range of K (m/s)	SBT I_c
1	Sensitive fine-grained	3×10^{-10} to 3×10^{-8}	NA
2	Organic soils – clay	1×10^{-10} to 1×10^{-8}	$I_c > 3.60$
3	Clay	1×10^{-10} to 1×10^{-9}	$2.95 < I_c < 3.60$
4	Silt mixture	3×10^{-9} to 1×10^{-7}	$2.60 < I_c < 2.95$
5	Sand mixture	1×10^{-7} to 1×10^{-5}	$2.05 < I_c < 2.60$
6	Sand	1×10^{-5} to 1×10^{-3}	$1.31 < I_c < 2.05$
7	Dense sand to gravelly sand	1×10^{-3} to 1	$I_c < 1.31$
8	*Very dense/stiff soil	1×10^{-8} to 1×10^{-3}	NA
9	*Very stiff fine-grained soil	1×10^{-9} to 1×10^{-7}	NA

4.2 Stream water quality evaluation

The result of some physical parameters of the water quality is presented in Table 7. The test was done in order to have an understanding of the nature of the water as it relates to concreting and reinforcement for civil engineering works. Acidic water, salts, organic matter, excess minerals, acids, etc., are usually damaging to concrete and its reinforcement [23]. This occurs during their reaction with concrete, leading to lower strength and corrosion of rebar (especially by chloride molecules). The temperature of the water varied from 27.5 °C to 28.8 °C, with an average (avg.) of 28.4°C. The SG ranged from 0.995 to 0.997, with an overall average of 0.9961. All the samples have SG values less than 1.000, signifying a freshwater type with less concentration of chlorides and acidic tendencies [45]. Nevertheless, there is significant overlap in the values in the samples from wells and boreholes.

The pH values fluctuated between 6.9 and 7.2 with an average of 6.99. This range of values is below the 6.5 acceptable standard limit for concreting water [45], since acidic water would react with concrete, dissolving its calcium component, breaking down the bond structure, resulting in intensification of porosity and corrosion of reinforcements [23].

EC indicates the level of dissolved ions, and varied from 89 µs/cm - 198 µs/cm, with an average of 127.89 µs/cm. These values are within 0 – 200 µs/cm specified for the fresh water group, hence the water would not have any negative impact on concrete structure, block molding, or setting. The sulfate values ranged between 32 and 73 mg/L, with an average value of 49.67 mg/L. The reaction of sulfate with concrete forms ettringite, which is an expansive crystal that causes unnecessary pressure on concrete, leading to cracks and disintegration. The maximum standard limit for sulfate is 1000 mg/L for SO_4 or 400 mg/L for SO_3. Thus, the values obtained are below these standards either as SO4 or SO_3 [46]. Salinity expresses the complete concentration of dissolved salt. The salinity of the water ranged from 0.011 to 0.023 % (avg. 0.01922%). Based on the obtained values, the value is below the maximum acceptable value of 1% for reinforced cement concrete. TDS values varied from 87 to 231 ppm, with an average of 160.33 ppm. The TDS defines all organic and inorganic constituents present in water, including sulfate and chlorides [47], [48]. High TDS can cause physical salt attack, i.e., salt crystallization within the pores of concrete, thereby reducing the compressive strength. TDS values below 500 ppm are usually safe for concrete structures and can increase their compressive strength early, but higher values can retard strength, reduce durability, and increase vulnerability for steel corrosion, especially if the chlorides of the water are high [45], [49]. The obtained values are within the acceptable threshold of 500 ppm for concreting and its reinforced steel.

4.3 Geotechnical Investigation

Table 8 summarizes the result of the geotechnical laboratory analysis, while Table 9 presents parameters derived from CPT data. The NMC ranged from 7.9 9 (quartzite) – 16.7 % (schistose quartzite) with an average (avg.) of 12.5. The engineering behaviour of soil is influenced majorly by the relative proportions of its constituent sizes present, grain shapes, and density of packing [46]. The grain size gives the relative amounts of the sizes of particles [50]. The percent gravel varied from 0 (schistose quartzite) – 3.84 % (quartzite) (avg. 0.6 %), % sand ranged from 37.29 (schistose quartzite) – 70.74 % (quartzite) (avg. 50.5 %), % silt is between 16.7 (quartzite) and 36.2 % (schistose quartzite) (avg. 27.4 %), and % clay varied from 10.6 (quartzite) – 35.8 % (schistose quartzite) (avg. 21.5 %). The proportion of clay (0.075 mm) and its mineralogy, and water content have a higher impact than its sizes in the engineering behaviour [46, 51-52]. Therefore, the % fines ranged from 28.3 (quartzite) – 62.7 % (schistose quartzite) (48.9 %). This implies that the soil has moderately low NMC, typical of well-drained soil [51]. The soil is coarse since the values of the sand/gravel is more than the fines component. However, the soil samples derived from quartzite showed better competence based relative low abundance of clay. Consequently, the soil is generally a mixture of sand, silt, and clay (SC-SM). The SG varied from 2.6907 – 2.7612 (quartzite) (avg. 2.7288). The consistency limits describes stability of soil in terms of firmness, stiffness, or softness of fine-grained soil in relation to water content [50]. Fine-grained soils usually contain clays and silts [51], therefore, the plasticity index of fine soil depends on the proportion of silt or clay in the soil. The LL ranged from 35.6 (quartzite) – 62.4 % (schistose quartzite) (avg. 50.9 %), PL varied from 22.6 to 38.7 % (schistose quartzite) (avg. 31.0 %), and PI varied between 8.8 (quartzite) – 32.9 % (schistose quartzite) (avg. 19.9 %). The MDD ranged between 1722 (schistose quartzite) to 1994 kg/m^3 (quartzite) (avg. 1849 kg/m^3), and OMC of 11.2 (quartzite) to 20.2 % (schistose quartzite) (avg. 17.3 %). High compaction in terms of MDD at low moisture content is very imperative in airfield construction to prevent serious consolidation under traffic or embankment weight [49].

Table 5. Hydro-geological Field Data

Sample No.	Well No./ Location	Easting	Northing	Elevation (m)	Depth to Water Level (m)	Total Depth (m)	Water Column (m)	hydraulic head (m)
S1	1 (SE)	078176	0799863	325	8.1	11.2	3.1	316.9
S2	2 (SE)	0783358	0799585	331	9.7	12.2	1.3	321.3
S3	3 (NE)	0782782	0799244	341	10.5	15.3	4.8	330.5

Table 6. Information Obtained on the Existing Boreholes within the Study Area

Sample No.	Borehole No.	Easting	Northing	Depth (m)	Condition Since When Dug
SL4	1	0782558	0799383	20	Very Productive
SL5	2	0782763	0799463	45	Very Productive
SL6	3	0782811	0799139	30	Fairly Productive
SL7	4	0783066	0799503	30	Fairly Productive
SL8	5	0782782	0799378	45	Fairly Productive
SL9	6	0782407	0800466	45	Less Productive

Table 7. Physical quality/parameters of the stream water during the dry and rainy seasons

Parameter/ Sample No.	T° (°C)	SG	pH	EC (μs/cm)	Sulfate (mg/L)	Salinity (%)	TDS (ppm)
SL2	28.6	0.995	7.0	123	32	0.011	124
SL2	28.5	0.996	6.9	142	45	0.023	143
SL3	27.9	0.995	6.9	198	66	0.020	87
SL4	28.5	0.997	6.9	121	73	0.022	231
SL5	28.8	0.997	7.1	151	51	0.021	143
SL6	28.6	0.995	7.2	89	64	0.011	123
SL7	28.5	0.997	6.9	98	45	0.021	221
SL8	27.5	0.996	6.9	105	39	0.021	176
SL9	28.6	0.997	7.1	124	32	0.023	195

The respective D_{10}, D_{30}, and D_{60} of the soil ranged from 0.0145 (schistose quartzite) – 0.0199 (quartzite) (avg. 0.015952), 0.0275 (schistose quartzite) – 0.08 (quartzite) (avg. 0.03752), and 0.075 (schistose quartzite) – 0.255 (quartzite) (avg. 0.151441), respectively. These represent the maximum particle size of the smallest 10 %, 30 %, and 60 % of the sample, respectively. The average of these values falls within the clay, silt, and fine sand boundaries, respectively. The coefficient of uniformity and curvature varied from 2.46 (quartzite) to 5.75 (schistose quartzite) (avg. 4.21), and 0.35 – 1.26 (quartzite) (avg. 0.5932). The values of Cu signify a uniformly graded soil since it's generally less than 6.0, with Cc between 1 and 3 [46], typical of sand or gravel dominated soil. The sand in hand specimens are angular to sub angular, hence a more grain interlock is expected under loading, with the fines serving as binding material within pores spaces [46]. This interlocking characteristics improves or increase strength and stiffness. This is one of the attributes requirement in roadworks as highly interlocking soil material provides more resistance against dislodgement with traffic [46], [49]. The unit weight varied between 18.34 (schistose quartzite) – 19.45 kg/m^3 (schistose quartzite) (avg. 18.92 kg/m^3). The CBR (drained) ranged from 6.8 (schistose quartzite) – 14.8 % (quartzite) (avg. 10.3 %). This values is above the minimum 10 % threshold for highway subgrade material according to Federal Ministry of Works and Housing of Nigeria [53]. The ministry recommends less than or equal to 10% for subgrade, 30% for sub-base and 80% for base course soil for road/highway construction. Thus, all the samples satisfy the condition for subgrade and sub-base material for road construction

The shear parameters of the soil gave cohesion values between 17 (schistose quartzite) – 29 kN/m^2 (schistose quartzite) (avg. 23.21 kN/m^2), and a friction angle of 24 (schistose quartzite) - 33° (schistose quartzite) (29.06°). This implies that there is more contribution to shear resistance of the soil from the angle of friction than cohesion, which consequently validates the sand dominance over the fines grains. The E_s ranged from 13600 (schistose quartzite) to 23200 kN/m^2 (schistose quartzite) (avg. 18715.15 kN/m^2), with expected elastic settlement of 26.2 (schistose quartzite) to 46.6 mm (schistose quartzite) (avg. 34.19 mm) for structural loading of magnitude 250 kN. The ultimate bearing capacity varied from 155 (schistose quartzite) to 194 kN/m^2 (quartzite) (avg. 172.61 kN/m^2), hence the soil is very competent to offer high resistance to shear failure [46]. The permeability and porosity ranged from 0.43 (schistose quartzite) to 0.55 (schistose quartzite/quartzite) (avg. 0.49), and 30.1 to 35.6 % (avg. 32.70 %). Drainage is a reflection of soil permeability, soil that retains water may cause an increase in pore water pressure, resulting reduction in strength [47]. Though sand and gravel permit rapid draining of water thereby also attract water in ingress. Soil's desirability properties for airfields or highways are good compaction, adequate strength, adequate drainage, acceptable compression or expansion, resistance to frost action, especially in regions where frost is an issue [22]. The EPA recommendation [45] of soil for liner material properties states a minimum of LL of 20 – 30 %, and PI of 10 – 30 %, and less than 1×10^{-7} m/s. High plasticity silt or clay is usually recommended with a minimum thickness of 0.5 m, and a friction angle of at least 12° to over 40°. Consequently, the soil does not satisfy these recommendations.

Nevertheless, coarse-grained soil would make a good subgrade, subbase material, and embankment material. Consequently, the soil would sufficed foundation pressure of 250 KN (even more) for buildings, bridges, and basement construction, with maximum compression less than 40 mm. A load of 250 kN/m² is a typical, safe, yet significant design bearing pressure for firm soil or shallow foundations, making it suitable to analyze settlement under near-maximum loading conditions. Using a solid, initial applied load like 250 kN allows engineers to predict the immediate deformation before consolidation occurs. It also aligns with typical, safe engineering loads for firm to dense clay/sand (such as 150-350 kN/m²) frequently used in foundation analyses. Consequently, this value is within the expected settlement for soil sand-silt-clay mixture. Compression or settlement of soil becomes an issue in design primarily when heavy fills are placed on compressive soils [54]. It should be noted that the expansion of soil increases with an increase in liquid limit; also, the structure, shape, and loading (previous) history play significant roles [46].

The results of the CPT with respect to refusal depths and all soil parameters derived from the CPT are presented in Tables 10 and 11, while typical curves are shown in the Appendix. The refusal depth for the soil ranged from 0.75 - 2.0 m with an average (avg.) of 0.98 m, hence, the specific refusal depth for the area is 2.0 m, signifying very high compacted subsoil at shallow depth. The obtained q_c varied from 82 – 201 kg/cm^2 (avg. 134.30 kg/cm^2), q_t ranged from 82 (schistose quartzite) – 201 kg/cm^2 (quartzite) (avg. 137.3 kg/cm^2), and the q_s ranged from 2 – 5 kg/cm^2 (avg. 3.36 kg/cm^2). The % R_f ranged from 1.76 – 3.76 (avg. 2. 42). The high magnitude of q_c values showed is the major component of soil bearing capacity to sustain and transmit the structural pressure through the soil layers to the bedrock. Most soil that recorded high q_c values is usually coarse-grained soil, unlike cohesive soil, which offers resistance to pressure based on sleeve friction. Hence, values of q_c values are higher in dense sand and gravel, but lower in clay and (plastic) silt. The q_c is generally between 8.24 – 20.2 MPa (avg. 14.01 MPa).

Table 8. Result summary of laboratory (geotechnical) parameters

Soil Parameter	Minimum	Maximum	Average
NMC	7.9	16.7	12.50
% Gravel	0	3.84	0.60
% Sand	37.29	70.74	50.50
% Silt	16.7	36.2	27.40
% Clay	10.6	35.8	21.50
% Fines	28.3	62.7	48.90
SG	2.6907	2.7612	2.7288
LL (%)	35.6	62.4	50.89
PL (%)	22.6	38.7	31.02
PI (%)	8.80	32.9	19.88
MDD (kg/m^3)	1722	1994	1849
OMC (%)	11.2	20.2	17.3
D_{10}	0.0145	0.0199	0.01595
D_{30}	0.0275	0.080	0.03752
D_{60}	0.075	0.255	0.15144
C_u	2.46	5.75	4.21
C_C	0.35	1.26	0.5952
CBR (%)	6.80	14.8	10.3
Cohesion (kN/m^2)	17	29	23.21
Friction Angle (°)	24	33	29.1
Allowable bearing capacity (kN/m^2)	155	194	172.6

Table 9. Result summary of derived geotechnical parameters from CPT data

Soil Parameter	Minimum	Maximum	Average
Porosity	30.1	35.6	32.68
Permeability	0.43	0.55	0.49
Unit weight (kg/m^3)	18.34	19.45	18.97
Allowable bearing pressure (square footing) (kN/m^2)	60.3	90.5	77.35
Ultimate bearing capacity (kN/m^2)	181	271.5	232.1
Si (mm)	26.2	46.6	34.19
Es (kN/m^2)	13600	23200	18715.15

The equivalent SPT-N values varied from 21 (schistose quartzite) to 50 (quartzite) (avg. 35), the friction angle ranged between 33.0 – 41.50 ° (37.12°), cohesion varied from 164.75 – 404.01 kPa (avg. 280 kPa), and unit weight between 19.97 – 21.34 kN/m^3 (20.66 kN/m^3 avg.). The SPT-N value indicates the soil strength and density based on the degree of stiffness [55] during penetration, with higher values corresponding to soil with high relative density, cohesion, angle of friction, and unit weight [35], [36]. This soil's parameters are essential for rating it for construction. The N-value increases with granular soil; the average value of 35 recorded corresponds to dense (tightly packed) soil material [37]. The average friction angle of 37.12° and cohesion (280.16 kPa) also signify competent well-compacted sand/gravel and fines mixtures, as the frictional angle and cohesion capacities are contributions from coarse and fines components of the soil, respectively. This also correlates with the grain size result obtained from the laboratory

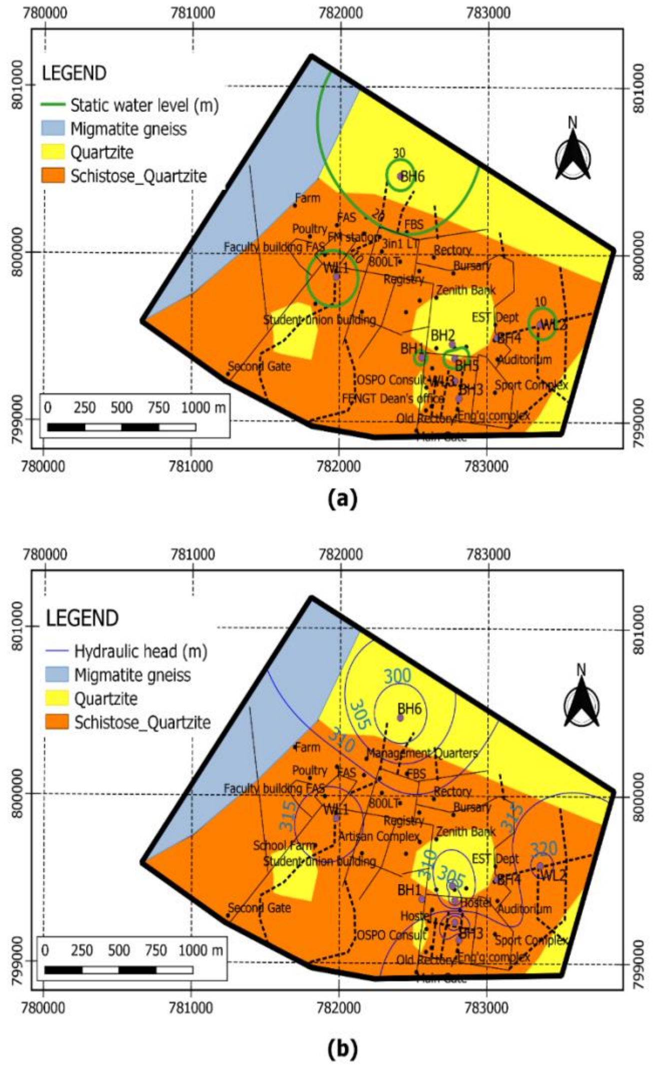

Fig. 4. (a) Spatial distribution of the static water level, and (b) hydraulic head across the study area

The unit weight obtained is generally higher than values for dry sand (13 – 20 kg/m^3), but within the range for saturated sand or mixed soil of significant fines [35]. Based on the obtained values qc, estimated N-SPT, and angle of friction, the state of packing of the soil using Table 12 can be classified as medium/dense soil of large relative density. The shear strength (undrained) values ranged from 573 (schistose quartzite) to 1404 kN/m^2 (schistose quartzite) with an average of 573 kN/m^2. The Su measures the maximum stress or pressure a soil can withstand in shear. Therefore, all the soil samples showed high shear resistance, with overlapping values for quartzite and schistose quartzite. The material index (Ic) connotes overall soil behaviour, as higher Ic signifies competent soil for foundation, pavement subgrade/subbase, and embankment construction [42].

Table 10. Result Summary of the CPT

Sample No.	Refusal Depth (m)	q_c (kg/cm²)	$q_c + q_f$ (kg/cm²)	q_f (kg/cm²)	R_f%	Q_{all}	Geology
CPT-1	1.0	128	131	3	2.01	75	Schistose quartzite
CPT-2	0.75	130	134	4	2.98	103	Schistose quartzite
CPT-3	2.0	201	206	5	2.55	129	Quartzite
CPT-4	1.0	128	131	3	2.01	67	Schistose quartzite
CPT-5	0.75	110	114	4	3.76	75	Schistose quartzite
CPT-6	0.75	125	129	4	2.87	88	Schistose quartzite
CPT-7	1.0	120	123	3	2.34	68	Schistose quartzite
CPT-8	1.75	180	184	4	1.98	84	Quartzite
CPT-9	0.75	128	133	5	3.72	101	Schistose quartzite
CPT-10	0.75	130	133	3	2.15	98	Schistose quartzite
CPT-11	2.0	100	103	3	2.60	46	Quartzite
CPT-12	2.0	100	103	3	2.71	38	Schistose quartzite
CPT-13	0.75	125	129	4	2.88	77	Quartzite
CPT-14	0.75	120	123	3	2.21	78	Schistose quartzite
CPT-15	1.0	124	126	2	1.88	66	Schistose quartzite
CPT-16	1.0	120	123	3	2.75	60	Schistose quartzite
CPT-17	1.0	120	123	3	2.24	65	Schistose quartzite
CPT-18	0.75	140	143	3	1.86	103	Quartzite
CPT-19	0.75	82	84	2	2.56	65	Schistose quartzite
CPT-20	1.0	180	184	4	2.02	106	Schistose quartzite
CPT-21	1.0	176	179	3	1.76	110	Schistose quartzite
CPT-22	0.75	130	133	3	2.26	86	Schistose quartzite
CPT-23	0.75	118	121	3	2.66	72	Schistose quartzite
CPT-24	0.75	125	128	3	2.22	82	Schistose quartzite
CPT-25	0.75	105	107	2	1.76	76	Schistose quartzite
CPT-26	0.75	120	123	3	2.11	71	Schistose quartzite
CPT-27	0.75	130	134	4	2.99	87	Schistose quartzite
CPT-28	0.75	118	121	3	2.44	73	Schistose quartzite
CPT-29	0.75	125	128	3	2.46	78	Schistose quartzite
CPT-30	0.75	118	121	3	2.40	71	Quartzite
CPT-31	1.0	186	190	4	2.25	99	Quartzite
CPT-32	1.0	198	203	5	2.30	115	Quartzite
CPT-33	1.0	192	196	4	2.31	117	Quartzite

The Ic varied from 2.18 to 2.58 (avg. 2.40), with average values of 2.42 and 2.39 for quartzite and schistose quartzite, respectively. The range of values showed that the samples fall within Zone 4 (94%), and Zone 5 (6%). This suggests that the soils are sand-silt mixtures (Table 4), which corroborates the grain analysis laboratory result.

4.4 Geoelectrical maps

The curve types acquired from the study area included KH (47.50 %), KHKH (7.5 %), H (11.25 %), HKH (16.25 %), QH (11.25 %), HK (2.50 %), AK (1.25 %), KQ (1.25 %), and Q (1.25 %). The KH is the most preponderant, and signifies the subsurface geology consisting of low resistivity topsoil overlying high resistivity subsoil (likely lateritic hardpan), followed by the high conducive weathered layer, and basement rock. This type of configuration is good for civil engineering construction with the removal of the topsoil [7], [10], [25], as it's usually stripped or removed for any civil engineering construction, especially pavement/airfield and embankment, due to the presence of organic matter, which can induce settlement leading to structural failure. The spatial distribution of the topsoil thickness (figure 5a) and resistivity (figure 5b) showed values ranging from 0.5 to 2.1 m and 300 – 1200 Ωm. The subsoil resistivity and thickness across the study area are shown in figure 6, with thickness varying from 5 – 10 m, and resistivity ranging between 250 and 1500 Ωm. The resistivity of the subsoil suggests clay-sand, sand, and laterite composition. Both the topsoil and subsoil are capable of sustaining structural load effectively with expected moderate settlement, due to the large thickness, especially at the southwestern flank. The depth of weathering, equivalent to overburden thickness or depth to basement rock (figure 7), showed a distribution ranging from 10 to 70 m, with the southern part showing relatively higher values. Areas with high depth of weathering would likely experience higher settlement than thin overburden areas. The northern part is also characterized with relative low resistivity values in the range of 400 – 1000 Ωm. The overburden thickness generally increases towards the south. Subsequently, the southeastern part showed higher competence in terms of the resistivity values. The topsoil thickness is generally uniform across the study area. However, the degree of compaction, temperature, mineral/salt content, soil type, and moisture content are factors influencing soil resistivity [46]. Even though the southeastern area seems to have better construction characteristics based on resistivity and thickness, as it portends to offer high resistance or bearing capacity to loading with less settlement, the area is generally competent with an average resistivity of 850 Ωm. Thus, the topsoil/subsoil would be less corrosive to metallic grounding systems (solar installation) without maintenance degradation [23].

The soil is capable of supporting and distributing structural loads (traffic loads) without much settlement, and maintaining drainage for a long-lasting road [24]. Embankment soil characteristics focus on soil's shear strength, settlement (stability), degree of saturation, and permeability. Thus, a well-graded material with good drainage and compaction is usually desired [12], especially granular soils, which are capable of resisting shear failure and landslide movement. In bridge construction, the requirement of the soil is strength in terms of shear, bearing capacity, compressibility or settlement, soil stiffness, and vibration or seismic responses (dynamic loading). These properties, if checked properly during the design and construction, would prevent failure, settlement, and provides or ensure good foundation stability [46].

4.5 Magnetic Susceptibility map

The aerial distribution of magnetic susceptibility across the area is shown in figure 8, with values ranging from -16064.55 to 1680.93 nT. The map shows the subsurface geology on the basis of variation in the earth's magnetic field intensity, which is a function of the magnetic properties of the underlying rocks. Igneous and metamorphic rocks generally contain a large proportion of magnetic minerals and are therefore more magnetic than sedimentary rocks. In general, the basic rocks are more magnetic than acidic rocks [9]. From the map, the northern part through the central to southeastern region is generally characterized by magnetic susceptibility material, corresponding to a schistose quartzite environment. Schistose quartzite is characterized by foliated texture with the occurrence of platy minerals. The low magnetic susceptibility in schistose quartzite is mainly induced by paramagnetic phyllosilicates [9], [46]. However, iron-bearing minerals such as biotite, magnetite, and amphibole usually increase the value of magnetic susceptibility from near-zero or zero to intermediate values. It can be noted from the map that areas underlain with quartzite also showed high magnetic susceptibility, like a schistose quartzite environment. Even though it is expected quartzite dominated area would have lower magnetic susceptibility than schistose quartzite. Quartzite, by reason of its primary mineral lithology, is composed of diamagnetic quartz, while schistose quartzite usually has low – intermediate positive magnetic susceptibility, depending on the amount or magnitude of trace amounts of ferromagnetic minerals (accessory) present [9]. Thus, the presence of impure materials such as magnetite/hematite by oxidation or environmental contamination can impact some degree of positivity or increase the magnetic susceptibility of quartzite. Hence, relatively high values recorded in the quartzite environment can be a result of environmental contamination and material oxidation by imported mineral matter [46]. Environmental contamination involving high magnetic material in quartzite regions is generally driven by the accumulation of anthropogenic magnetic particles, such as industrial fly ash, magnetic spherules from industrial processes, or heavy metal pollution, which exhibit high magnetic susceptibility compared to the natural, low-magnetic background of quartzite rocks.

4.6 Geochemical Analysis

Geochemical analysis of the soil samples across the study area is presented in Tables 13 and 14 for elemental and mineral compositions, respectively. The values recorded for Cu ranged from 0.21 – 0.31 ppm (0.25 ppm avg.), Fe varied from 0.17 – 0.26 ppm (0.21 avg.), Mn ranged between 0.12 – 0.30 ppm (0.20 ppm avg.), Zn values are between 0.57 to 0.91 ppm (0.74 ppm avg.), Pb ranged from 0.14 – 0.23 ppm (0.20 ppm avg.), As varied from 0.03 – 0.26 ppm (0.08 avg.), Na ranged between 7.0 – 13.0 ppm (10.0 ppm avg.), K values are between 12 and 22 ppm (18.40 ppm avg.), Si ranged from 19.0 – 29.0 ppm (24.50 ppm avg.), and Ca varied from 21.0 – 34.0 ppm (27.10 ppm avg.). The results revealed that (in order of abundance) Ca, Si, K, and Na are the most dominant elements, while Zn, Cu, Fe, Mn, Pb, and As are the accessory elements. The major mineral oxides tested for, have values ranging from 16.50 – 47.60 ppm (36.58 ppm avg.) for CaO; 14.50 – 26.50 ppm (22.18 ppm avg.) for K2O; 9.40 – 17.50 ppm (13.46 ppm avg.) for NaO; 40.60 – 62.0 ppm (52.41 ppm avg.) for SiO2; 0.71 – 1.13 ppm (0.92 ppm avg.) for ZnO; 0.27 – 0.39 ppm (0.31 ppm avg.) for CuO; 0.15 – 0.24 ppm (0.20 ppm avg.) for PbO2; 0.22 – 0.34 ppm (0.27 ppm avg.) for FeO; 0.15 – 0.39 ppm (0.26 ppm avg.) for MnO; and 0.04 – 0.34 ppm (0.10 ppm avg.) for AsO. The major mineral oxides are (in descending order) SiO2, CaO, K2O, and NaO, as they constitute more than 90 %. The abundance of these major mineral oxides in the soil samples signifies the nature of the parent rock (schistose quartzite/quartzite). Soils with relatively high concentrations of these elements demonstrate distinctive properties that have effects on the soil structure for civil engineering construction [13], [46]. The abundance of SiO2 content of the samples implies better engineering properties, translating to high CBR, shear strength, improved compaction characteristics, and lower plasticity/swelling potential [46]. The high CaO can help mitigate some of the deleterious structural impacts of NaO by helping with flocculation. The NaO can also act as an alkaline activator to stabilize or steady the silt soil and increase the mechanical attributes and durability of cement-like materials for construction [49], by forming stable calcium silicate hydrates, which would reduce water absorption/permeability and other environmental stressors. Thus, the soil is balanced, in terms of its mineralogy, as it can sustain structural load without any deleterious effects of its elements as subgrade, subbase, or base material in highway construction. The soil material is capable of producing strong, durable cementitious binders by chemical reaction, resulting in soil stabilization [55]. The SiO_2 in reactive form is a critical pozzolanic material. In reaction with CaO and water, the SiO_2 forms additional cementitious material, which would further strengthen and make the soil more durable than when these minerals are not present. Consequently, the soil is in a stabilized form.

Table 11. Result Summary of Parameters derived from CPT

Sample No.	Refusal Depth (m)	Qc (MPa)	Equiv. N-Value	Friction angle	Cohesion	Unit weight (kN/m^2)	I_C	S_U (KN/m^2)
CPT-1	1.0	12.85	32	36.30	256.94	20.48	2.43	895
CPT-2	0.75	13.14	33	36.51	262.82	20.51	2.28	909
CPT-3	2.0	20.20	50	41.55	404.04	21.79	2.46	1404
CPT-4	1.0	12.85	32	36.30	256.96	20.92	2.43	895
CPT-5	0.75	11.18	28	35.11	223.59	20.92	2.21	769
CPT-6	0.75	12.65	32	36.16	253.01	21.14	2.27	874
CPT-7	1.0	12.06	30	35.73	241.25	20.97	2.40	839
CPT-8	1.75	18.04	45	40.00	360.89	21.60	2.50	1258
CPT-9	0.75	13.04	33	36.44	260.86	20.67	2.18	895
CPT-10	0.75	13.04	33	36.44	260.86	20.82	2.41	909
CPT-11	2.0	13.91	35	37.05	278.12	20.98	2.48	697
CPT-12	2.0	11.18	28	35.11	223.60	20.48	2.48	697
CPT-13	0.75	20.20	51	41.55	404.04	21.79	2.27	874
CPT-14	0.75	12.06	30	35.74	241.25	20.92	2.37	839
CPT-15	1.0	12.36	31	35.95	247.13	20.98	2.58	867
CPT-16	1.0	12.06	30	35.74	241.25	20.96	2.40	839
CPT-17	1.0	12.06	30	35.74	241.25	20.98	2.40	839
CPT-18	0.75	14.02	35	37.14	280.47	21.23	2.44	979
CPT-19	0.75	8.24	21	33.01	164.75	20.43	2.39	573
CPT-20	1.0	18.04	45	40.01	360.89	21.65	2.43	1259
CPT-21	1.0	17.55	44	39.66	351.08	21.63	2.55	1231
CPT-22	0.75	13.04	33	36.44	260.85	21.19	2.41	909
CPT-23	0.75	11.87	30	35.60	237.32	21.06	2.37	825
CPT-24	0.75	13.13	33	36.50	262.62	21.10	2.39	874
CPT-25	0.75	8.24	21	33.00	164.75	20.43	2.49	734
CPT-26	0.75	18.04	45	40.01	360.89	21.65	2.37	839
CPT-27	0.75	13.14	33	36.51	262.82	21.23	2.28	909
CPT-28	0.75	11.87	30	35.60	237.32	21.09	2.37	825
CPT-29	0.75	12.55	31	36.09	251.05	21.19	2.39	874
CPT-30	0.75	11.87	30	35.60	237.32	21.12	2.37	825
CPT-31	1.0	18.63	47	40.43	372.66	21.83	2.45	1301
CPT-32	1.0	19.91	50	41.34	398.15	21.95	2.37	1385
CPT-33	1.0	19.22	48	40.85	384.42	21.91	2.46	1343

Table 12. Correlation of Qc and relative density with friction angle for cohensionless soils [35]

State of packing	Relative Density	SPT N	Qc in MPa	Approximate triaxial friction angle (degree)
Very loose	<0.2	<4	<2	<30
Loose	0.2 – 0.4	4 – 10	2 – 4	30 - 35
Medium dense	0.4 – 0.6	10 – 30	4 – 12	35 – 40
Dense	0.6 – 0.8	30 – 50	12 – 20	40 – 45
Very dense	>0.8	>50	>20	>45

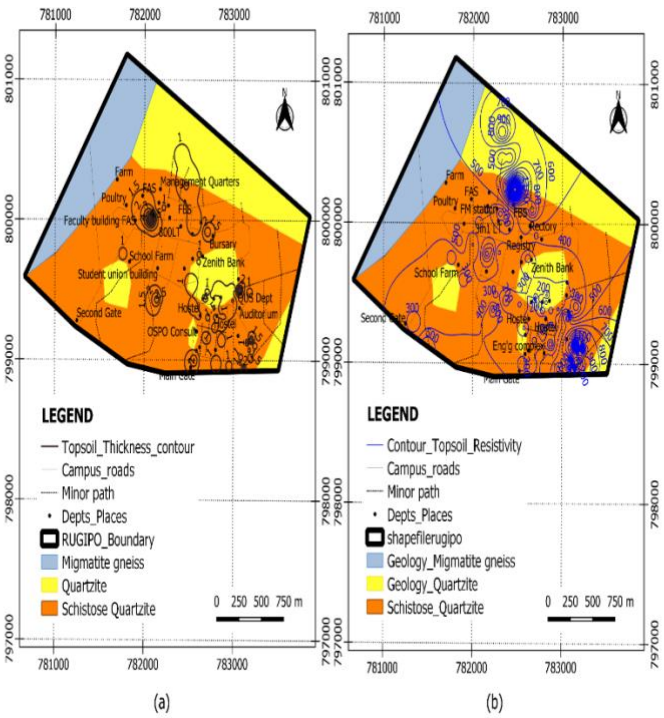

Fig. 5. Spatial distribution of (a) topsoil thickness, (b) Topsoil resistivity across the study area

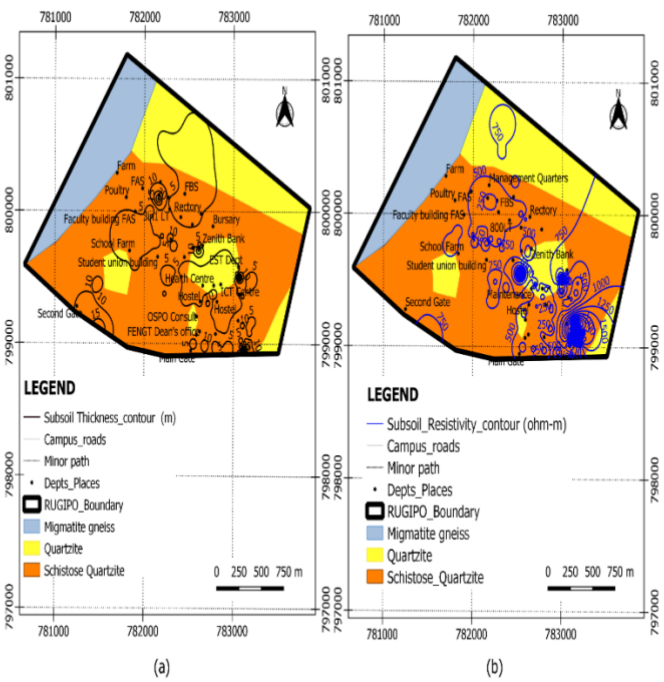

Fig. 6. Spatial distribution of (a) subsoil thickness, (b) subsoil resistivity across the study area

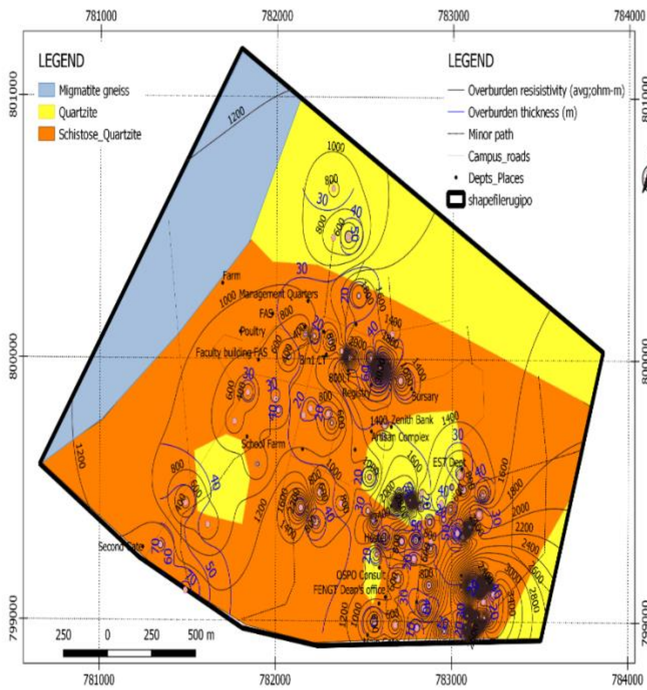

Fig. 7. Spatial distribution of overburden thickness and resistivity across the study area

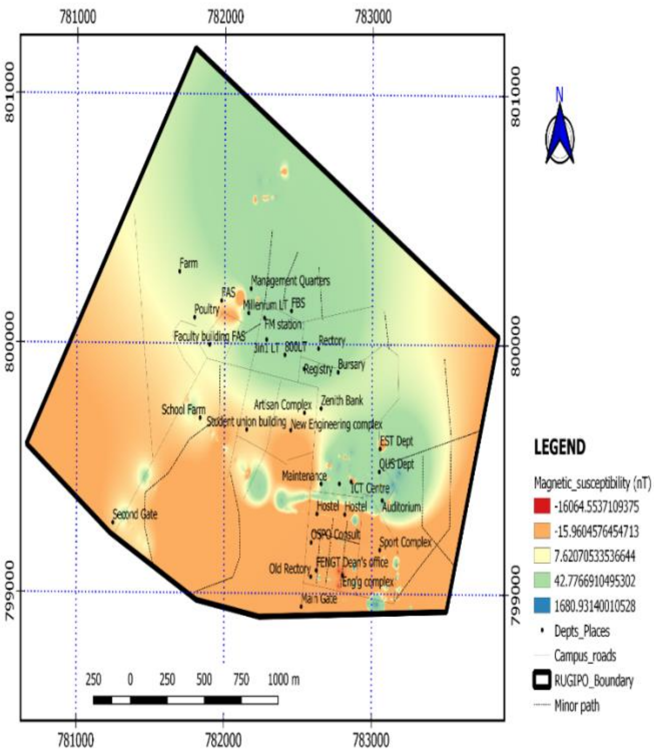

Fig. 8. Spatial distribution of the magnetic susceptibility across the area

Table 13. Summary of the relative quantity of Elements in the soil samples

	Cu (ppm)	Fe (ppm)	Mn (ppm)	Zn (ppm)	Pb (ppm)	As (ppm)	Na (ppm)	K (ppm)	Si (ppm)	Ca (ppm)
Average	0.25	0.21	0.20	0.74	0.20	0.08	10.00	18.40	24.50	27.10
Minimum	0.21	0.17	0.12	0.57	0.14	0.03	7.00	12.00	19.00	21.00
Maximum	0.31	0.26	0.30	0.91	0.23	0.26	13.00	22.00	29.00	34.00

Table 14. Summary of Relative quantity of Minerals in the soil samples

	CaO (ppm)	K_2O (ppm)	NaO (ppm)	SiO_2 (ppm)	ZnO (ppm)	CuO (ppm)	PbO_2 (ppm)	FeO (ppm)	MnO (ppm)	AsO (ppm)
Average	36.68	22.18	13.46	52.41	0.92	0.31	0.20	0.27	0.26	0.10
Minimum	16.80	14.50	9.40	40.60	0.71	0.27	0.15	0.22	0.15	0.04
Maximum	47.60	26.50	17.50	62.00	1.13	0.39	0.24	0.34	0.39	0.34

4.7 Petrology

Schistose quartzite (figure 9) and quartzite (figure 10) are the two major rock units in the study environment. The schistose quartzite has developed conspicuous and pronounced cleavage/planar foliation, though many occurred highly weathered. The cleavage/foliation is the result of the parallel arrangement of platy minerals, commonly clays, muscovite, biotite, chlorite, and sericite [9]. Also often present and in parallel arrangement are tabular or elongate clusters of other minerals, usually quartz and feldspars, and occasionally amphiboles. The foliation is a product of shear stresses imposed over long episodes of geological time on previous rocks like igneous or "high-grade" metamorphic rocks. The schistose can also be from sedimentary rocks such as siltstone, mudstone, or shale.

The engineering strength of schistose quartzite rocks is in the range of very weak to medium strength (20 - 60MPa), depending on the angle of schistocity relative to the applied load, and the presence of joints and discontinuities [46]. Schists having abundant quartz (SiO_2) are normally medium strong or strong, as they are very resistant to weathering, while greenschists rich in chlorite are usually very weak and susceptible to weathering. The most significant engineering characteristic of schistose rocks is their pronounced anisotropy [9], caused by the cleavage or foliation. The weathering product of the schistose quartzite varied slightly across the study area, as some areas are rich in micaceous minerals (such as muscovite, biotite, or chlorite), which tend to form micaceous silty or clayey soils when extremely weathered [56]. The silty/clay varieties are frequently of low in situ density and are vastly erodible by water or wind. Also, they are capable of being hydrophobic, making dust control challenging on construction sites, due to abrasion during handling and trafficking. Micaceous (minerals) silty soils, which contain significant amounts of mica minerals (often due to weathered metamorphic rocks), are known for their problematic engineering behavior, including a natural resistance to absorbing water, a phenomenon known as hydrophobic nature or soil water repellency. When disturbed during active construction, these soils present severe dust control challenges because conventional water spraying techniques are rendered ineffective. During active construction, such as excavation, earthwork, and vehicular traffic, breaks down micaceous particles, exacerbating the generation of fine, dry dust particles that easily become airborne.

Suitability of schistose rocks for use as filter materials, concrete aggregates, and pavement materials depends on the abundance or proportion of quartz, feldspar, or feldspathoid to the micaceous minerals. However, highly rich mica-rich schists are generally unsuitable for any of these purposes due to the very flaky shapes of the crushed materials and inadequate strengths of the particles, though they can be successfully used as rock fill. The schistose quartzite is also characterized by minor faults and joints parallel to the foliation. Land sliding is relatively common on slopes underlain by schistose rocks. However, in most of these, likely, the low shear strength of the schistose rocks along their foliation surfaces has contributed to the development of slope failure [57], [58].

The quartzite rock is not as widespread as the schistose quartzite in the study area. The quartzite is mostly made up of interlocking (recrystallized) quartz grains that are closely packed, resulting in an extremely dense/hard rock [46]. Feldspar, mica, and pyrite are commonly found as accessory minerals in hand specimens. Most of them had weathered, and some appeared as low-lying rock blocks or boulders. Weathering has attacked micaceous minerals, causing fracture and disintegration into a clay-silt-sand soil combination in areas where extensive weathering has occurred. The silica content is durable and remains intact, sustaining the rock's topography and eventually creating secondary minerals such as kaolinite and Fe-oxide. Physical weathering in quartzite is sluggish due to the lack of planes and cracks, as well as quartz's resilience at low temperatures [9]. Therefore, based on the stability of quartz and its hardness, they have high compressive strength (150 to over 350MPa), resistance to acidic weathering, low porosity, high density (2336 – 2641 kg/m^3), and excellent abrasion resistance [46]. Consequently, they are good and durable for foundation and aggregate constructions. Although its strength variability depends on metamorphic grade, the interlocking quartz mineral. The strike and dip of the foliation planes measured on both outcrops varied across the study area, as shown in figure 11. The foliation planes are formed by intense regional tectonic pressure (differential pressure), oriented in different directions. The rose diagram [59], [60] showed a prominent NE – SW and NW–SE direction (figure 11a), and the direction of the joints conforms with the measured foliations, as they are parallel to the regional foliation. The numerous orientations of the foliation and joints/fractures suggest differently oriented tectonic forces through the evolution of the structures. In addition, it implies that the different foliations and joints/fractures were produced at different geological times. The N-S and NE-SW structures are presumably associated with the Pan-African orogeny (600 MA ago), while pre-Pan-African (Eburnean) structures are oriented differently (especially in E – W or NW – NE trends) to these directions in the basement. Nevertheless, the Pan-African orogeny, as a later and presumably the last tectonic event in the basement, reconfigured and obliterated earlier structures. The dip of the planes forms one major cluster with a fairly steep slope (figure 11b), while the tight cluster of poles indicates that the foliation planes are parallel/near parallel. The implications of these foliation directions are, if the building's load is applied parallel to the foliation, it risks slip-planes forming, leading to differential settlement. Ideally, large structures are oriented so that the loads are distributed across the trend or perpendicular to the bedding to ensure maximum rock competence. A NE-SW foliation means that foundations designed for the site must account for anisotropic strength i.e., the rock is stronger in some directions than others. The foliation are not steeply dipping, which can cause building foundation loads to trigger sliding along these planes, resulting in uneven sinking. In addition, foliation planes act as natural pipelines for groundwater movement. A NE-SW and N-S trends might allow water to travel easily in that direction, potentially causing unexpected saturation or erosion underneath a building that disrupts that flow, leading to structural instability or high uplift pressures

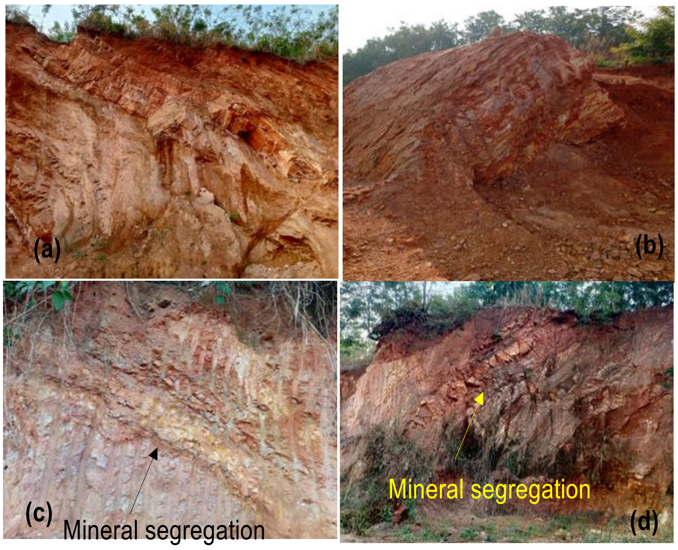

Fig. 9. Exposure of schistose quartzite, showing (a and b) strongly foliated with visible layers or bands of platy parallel mica flakes and mineral segregation (quartz band); (c and d) the rock is rich in quartz and mica (muscovite/biotite)

Fig. 10. (a – d) Exposure Quartzite ridge; (a and b) showing different joints/fractures orientation; and (d) disintegrated samples

The dominant strike and dip of the foliation plane are between 141° and 150°, and 051° and 060°, respectively, and this accounts for 33 % and 18.5 % accordingly, of the data acquired. The joints measured are generally closely spaced with a general trend in conformity with the foliation planes (figure 11c) observed on schistose quartzite. The joints generally dip to the west with a dominant range of 70 - 82°. The foliation plane is a plane of weakness and a key source of anisotropy in rock mass because its mechanical characteristics, such as deformability, strength, and stiffness, change with the direction of applied stress [46], [61]. The direction of foliation planes has a significant impact on slope stability, both natural and artificial. If the foliation descends toward an excavation, it might cause sliding or toppling failure along these weak planes, necessitating particular stabilizing measures such as rock bolts or retaining walls [62], [63], [64]. Furthermore, foliation planes can serve as conduits for groundwater movement since their permeability is typically significantly higher than that of the entire rock matrix. Understanding this is essential for dewatering activities during construction. The spacing and continuity of rocks determine their appropriateness for engineering building (as aggregate, dimension stones, and foundation). Rock with extensive, closely spaced foliation may be more brittle and susceptible to fragmentation. Under large loads, these planes may also collapse due to shear or differential settling.

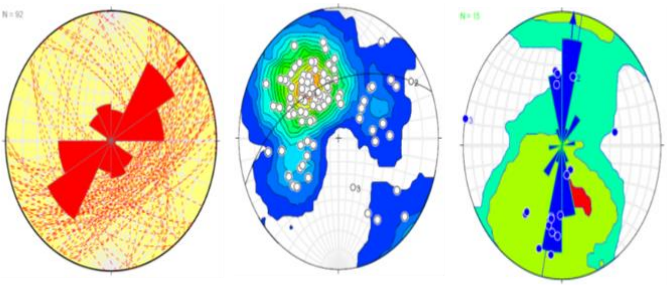

Fig. 11. Stereographic projection of the Foliation Planes (a) Great circle and rose diagram (b) Contour diagram (c) projection of the Joints

5. CONCLUSION

In this study, integrated methods have been deployed in evaluating the geomaterial (soil, rock, and water) in RUGIPO in relation to their uses for building foundation, reinforced cement concrete structure, pavement, and embankment construction, excavation/mines, and landfill. From the study, the following can be concluded:

1. The rock units in the area are schistose quartzite and quartzite, which are capable of providing (compressive) strength of 150 to over 350MPa, and 20 – 60 MPa, respectively. The quartzite will provide any support for any civil engineering construction, as it is characterized with less joints/fractures or discontinuities. The schistose quartzite for use as filler materials, concrete aggregates, embankment, and pavement, depends on the abundance of quartz, feldspar or feldspathoids to the micaceous minerals, and the presence of discontinuities.

2. SiO_2, CaO, K_2O, and NaO constitute 90% of the soil constituents. The abundance of SiO_2 (52.4 %) implies a good engineering tendency that can translate to high CBR, shear strength, and PI, and low compressibility/swelling potential.

3. The soils across the area are dominated by sand - silt mixture, with good geotechnical characteristics, in terms of average CBR (> 10%), cohesion (23.2 kN/m^2), friction angle (29.1°), PI (< 20 %), allowable bearing capacity (172.6 kN/m^2), modulus of elasticity (18715 kN/m^2), soil behaviour index (2.40), and elastic settlement (34.19 mm for more 250 kN load). Hence, the soil is expected to have good applications in basement or foundation, bridge, reinforced cement concrete structures (including slabs, lintels, and columns), pavement, and embankment. However, the soils fail in major properties for landfill/liners application in terms of PI, permeability, and porosity. Landfill liner sites require materials with very low permeability to prevent leachate from contaminating groundwater, typically using clay or synthetic materials, with specific geotechnical standards for permeability (≤1×10-7 cm/s) and porosity (0.2 – 0.3). Therefore the soil failed in these properties due to elevated values of porosity and permeability However, residual soil from a quartzite environment has better geotechnical properties than schistose quartzite.

4. The subsoil showed high resistance values (more than 500 Ωm), capable of accommodating burial of utilities and metallic grounding systems, such as communication mast, buried transmitter, electrical wiring system, etc.

5. The groundwater level is higher than 8 m across the study area. This average depth cannot threaten the basement/foundation structure. The quality of the water is within the recommended threshold for all the parameters tested, including T°, SG, pH, TDS, EC, salinity, sulfate, and EC.

However, the soil would require some degree of stabilization, such as chemical stabilization (cement/bitumen or bentonite) or grading the soil with more fines for liner's application. The best stabilization method for sand dominated soil, particularly when used as liners to reduce permeability and increase strength, involves chemical stabilization with cement or bentonite-slurry mixing. For environmental liners specifically, adding bentonite to sand effectively reduces permeability by filling pore spaces, while cement provides high strength for structural applications. Secondly, the orientation of foliation planes heavily influenced the stability of natural and excavated slopes, either in road cuts or open-pit mines [58], [59], [62], [63], [64], [65], [66]. During excavation, the dip of the planes (in schistose quartzite: 51 to 60°) should not be allowed to dip towards the excavation. This action can enhance sliding or toppling failure along these weak foliation planes. And in case this phenomenon is non-avoidable, then stabilization such as rock bolts and [66] or retaining walls can be used.

ACKNOWLEDGEMENT

The authors express their appreciation to TETFund Nigeria for providing grant through TETF/DR&D/CE/POLY/OWO /IBR/2022/VOL.II that has greatly assisted this study. The authors also appreciated the efforts of Mr Ajayi Gidi of geophysics Department of FUTA, Mr Ololade of Geology Department AAUA, Mr Ajayi of Geology Department EKSU, and Mr Bamidele (Lagos) for helping in geophysical surveys and CPT data acquisition.

REFERENCES

[1] O. O. Falowo, "Subsoil Condition and Development of Geo-Data Set for Effective Design, Construction and Management of Engineering Structures in Ondo Metropolis, Southwestern Nigeria" Malaysian Journal of Science and Advanced Technology, 3 (1) 48-71, 2023. doi: https://doi.org/10.56532/mjsat.v3i1.151

[2] S. Bayode, and A. A. Egbebi, "Subsoil Characterization for Foundation Stability Using Geophysical and Geotechnical Methods," Journal of Environment and Earth Science. Vol.10, No.6, 2020.Pp. 8, 2020, doi: https://doi.org/10.7176/jees/10-6-08

[3] O. O. Osinowo, and M. O. Falufosi, "3D electrical resistivity imaging (ERI) for subsurface evaluation in pre-engineering construction site investigation" NRIAG J Astro Geophys, 2018.

[4] A. O. Ibrahim, and P. O. Falae, "Integrated Geophysical and Geotechnical Methods for Pre-Foundation Investigations. Journal of Geology & Geophysics" 8:1, 2018, doi: https://doi.org/10.4172/2381-8719.1000453

[5] G. M. Olayanju, K. A. Mogaji, H. S. Lim, and T. S. Ojo, "Foundation integrity assessment using integrated geophysical and geotechnical techniques: Case study in crystalline basement complex, southwestern Nigeria" J Geophys Eng 2017, 14: 675- 690.

[6] L. Adeoti, A. O. Ojo, R. B. Adegbola, and O. O. Fasakin, O. O. "Geoelectric assessment as an aid to geotechnical investigation at a proposed residential development site in Ilubirin, Lagos, Southwestern Nigeria" Arab J Geosci 9: 338, 2016.

[7] O. J. Akintorinwa, and S. T. Oluwole, "Empirical relationship between electrical resistivity and geotechnical parameters: A case study of

Federal University of Technology campus, Akure SW, Nigeria" NRIAG J Astronomy Geophys 7: 123–133, 2018.

[8] S. A. Adejumo, A. O. Oyerinde, and M. O. Akeem, "Integrated geophysical and geotechnical subsoil evaluation for pre-foundation study of proposed site of vocational skill and entrepreneurship center at the polytechnic, Ibadan, SW, Nigeria" Int J Sci Eng Res (2015) 6: 910-917.

[9] C. C. Plummer, M. David, and H. G. Diane. "Physical Geology" (3rd Ed.), 119 p., 2001.

[10] O. I. Adewuyi, and O. F. Philips, "Integrated Geophysical and Geotechnical Methods for Pre-Foundation Investigations," J. Geol. Geophys. 8: 453, 2018. doi: https://doi.org/10.4172/2381-8719.1000453

[11] O. O. Falowo, O. Olorunda, T. Ologan, and A. Ayetoro, "Baseline Geo-Engineering Dataset and Parameters' Empirical Modeling for Civil Engineering Construction in Okeigbo, Southwestern Nigeria" International Journal of Earth Sciences Knowledge and Applications, Ataturk University, Turkey, 5 (2): 182-207, 2023. url: http://www.ijeska.com/index.php/ijeska

[12] GEM-12, "Guidelines for Embankment Construction. Geotechnical Engineering Manual": Revision #4, State Of New York Department Of Transportation, Geotechnical Engineering Bureau. August 2015.

[13] A. Asghar, W. Hussain, S. Ali, M. Hasnain, M. Ali, M. Obaidullah, "Evaluation of Geotechnical Properties and Petrographic Characteristics of Sandstone, Bagh Area, Azad Jammu and Kashmir, Pakistan". Geological Behaviour 7(1): 01-09, 2023.

[14] O. L. Ertugrul, and F. D.Canogullari, "An investigation on the geomechanical properties of fiber reinforced cohesive soils" Turkish Journal of Engineering, 5(1), 15–19, 2021.

[15] R. D. Holtz, W. D. Kovacs, and T. C. Sheehan, "An Introduction to Geotechnical Engineering", 2nd Edition, Pearson Publishing: 853 pages, 2011.

[16] M. S. B. A. Abd El-Karim, O. A. Mosa El Nawawy, and A. M. Abdelalim, "Identification and assessment of risk factors affecting construction projects" HBRC Journal, 13(2), 2017, 202–216. doi: https://doi.org/10.1016/j.hbrcj.2015.05.001

[17] A. Abd-Elhamed, H. E. Amin, and A. M. Abdelalim, "Integration of Design Optimality and Design Quality of RC buildings from the perspective of Value Engineering", International Journal of Civil and Structural Engineering Research, 2020: Vol. 8(Issue 1), pp.:105-116.

[18] N. A. Mohamed, A. M. Abdel-Alim, H. H. Ghith, and A. G. Sherif, "Assessment and Prediction Planning of R.C Structures Using BIM Technology", Journal of Engineering Research, 2020, 167, 48–56. doi: https://doi.org/10.21608/erj.2020.145845

[19] E. Yousri, A. E. B. Sayed, M. A. M. Farag, and A. M. Abdelalim, "Risk Identification of Building Construction Projects in Egypt", Buildings, 13(4), 1084, 2023. doi: https://doi.org/10.3390/buildings13041084

[20] I. G. Chendo, and N. I. Obi, "Building collapse in Nigeria: the causes, effects, consequences and remedies", International Journal of Civil Engineering, Construction and Estate Management, 3(4), pp.41–49, 2015.

[21] P. A. Adebowale, M. D. Gambo, I. A. Ankeli, and I. D. Daniel, "Building Collapse in Nigeria: Issues and Challenges", Conference of the International Journal of Arts & Sciences, 9(1), pp. 99–108, 2016.

[22] S. L. Hendarsin, "Practical Guide of Geotechnical Engineering Investigations for Civil Engineering Building Planning", Dept. of Civil Eng., Politeknik Negeri Bandung, Bandung (in Indonesian), 2003.

[23] K. Bourenane, A. B. D. Haddar, A. Haddar, I. Zerouki, and D. Abdessemed, "Monitoring and inspection to combat corrosion of pipeline lines in an oil field", Algerian Journal of Environmental Science and Technology December edition. 2023, Vol.9. No4., 5pp.

[24] R. Amer, A. Saad, T. A. Elhafeez, H. E. Kady, and M. Madi, "Geophysical and Geotechnical Investigation of Pavement Structures and Bridge Foundations", Austin J Earth Sci. 2014;1(1): 6.

[25] F. O. Eebo, A. B. Samuel, and G. M. Olayanju, "Geophysical and Geotechnical Investigations for Subsoil Competence at a Proposed Hostel Site at Oba Nla, Akure Southwestern Nigeria", Journal of Engineering Research and Sciences, 2022, 1(2): 41-49.

[26] A. Rungroj, and E. E. Mark, "Application of 2D electrical resistivity tomography to engineering projects: Three case studies", Songklanakarin J Sci Technol 37: 675-681, 2015.

[27] A. O. Fajana, O. G. Olaseeni, O. E. Bamidele, and O. P. Olabode, "Geophysical and geotechnical investigation for post foundation studies, Faculty of Social Sciences and Humanities, Federal University Oye Ekiti", FUOYE J Eng Tech 1: 2579-0617, 2016.

[28] O. O. Falowo, and M. B. Amodu, "Engineering Subsoil Characterization for Shallow Foundation Design in Ode Irele Area of Ondo State, Southwestern Nigeria", European Journal of Environment and Earth Sciences. Vol 1 (2), 2020, Pg.1, doi: https://doi.org/10.24018/ejgeo.2020.1.2.6

[29] M. P. Iloeje, "A New Geography of Nigeria.Longman": Nigeria. 26 – 28, 1981.

[30] N. G. Obaje, "Geology and mineral resources of Nigeria." Lecture Notes in Earth Sciences, Springer, Berlin, Heidelberg 120, 2009.

[31] British Standards Institution, "British Standard Methods of Test for soils for Civil Engineering Purposes" B.S 1377: Part 2, 1990.

[32] ASTM-D5778-07, "Standard test method for performing electronic friction cone and piezocone penetration testing of soils" ASTM International, West Conshohocken, PA, 2007. url: http://www.astm.org

[33] Canadian Geotechnical Society, "Canadian Foundation Engineering Manual", Third Edition, BiTech Publishers, Vancouver, BC: 512 p., 1992.

[34] J. G. Trofimenkov, "Penetration testing in the USSR" Proceedings 1st European Symposium on Penetration Testing (ESOPT), Vol. 1, Swedish Geotechnical Society, Stockholm:147-154, 1974.

[35] P. W. Mayne, "Geoengineering Design Using the Cone Penetration Test", Published by ConeTec Inc., Richmond, BC, Canada: 155 p., 2009. url: http://www.conetec.com

[36] T. Lunne, P. K. Robertson, and J. J. M. Powell, "Cone Penetration Testing in Geotechnical Practice", Routledge/Blackie Academic, London: 312 p., 1997.

[37] B. M. Lehane, "Relating foundation capacity in sands to CPT qc" Geotechnical & Geophysical Site Characterization, Vol. 1 (Proc. ISC-4, Pernambuco, Brazil), Taylor & Francis Group, London: 63-81, 2013.

[38] B. H. Fellenius, and A. Altaee, "Stress and settlement of footings in sand. Vertical and Horizontal Deformations of Foundations and Embankments", Vol. 2 (GSP 40), ASCE, Reston, VA, 1760-1773, 1994.

[39] P. K. Robertson, "Soil behaviour type from the CPT": an update. 2nd International Symposium on Cone Penetration Testing, CPT'10, Huntington Beach, CA, USA, 2010. url: http://www.cpt10.com

[40] R. Arbianto, T. Yuono, and Gunarso, "Comparison of California Bearing Ratio (CBR) Value Based on Cone Penetration Test (CPT) and Dynamic Cone Penetrometer (DCP)" Journal of Advanced Civil and Environmental Engineering Vol.4, No.2, 2021, pp 70-78

[41] C. K. Pen, "An assessment of the available methods of analysis for estimating the elastic moduli of road pavements", in Proc. 3rd Int. Conference on Bearing Capacity of Roads and Airfields, Trondheim. Huang, Y. H. 2004. Pavement Analysis and Design, Prentice-Hall, Englewood Cliffs, NJ, 1990.

[42] S. Eslaamizaad, and P. K. Robertson, "Cone penetration test to evaluate bearing capacity of foundations in sand", Proc. 49th Canadian Geotechnical Conference: Frontiers of Geotechnology, Vol. 1, St. Johns, Newfoundland: 429-438, 1996.

[43] J. A. Schneider, and J. N. Hotstream, "Cone Penetrometer Comparison Testing", Wisconsin DOT Final Report 10-10 prepared by Univ. Wisconsin, Madison: 298 pages, 2010.

[44] B. Yilmaz, and M. Turkoz, "Determination of shear strength parameters of compacted high plasticity clay soils based on different laboratory tests", Turkish Journal of Engineering, 2022, 6(4), 313–319.

[45] C. W. Fetter, "Applied Hydrogeology", Prentice-Hall, Inc. Upper Saddle River, New Jersey, USA, 615pp, 2001.

[46] D. G. Price, "Engineering Geology: Principles and Practice", Springer-Verlag Berlin Heidelberg, 460pp, 2009.

[47] M. Thangarajan, "Groundwater: Resource Evaluation, Augmentation, Contamination, Restoration, Modeling and Management", Springer publication, 7/28, Mahaveer Street, Ansari Road, Daryaganj, New Delhi, 110 002, India, 2007.

[48] A. S. Al-Ameeri, M. I. Rafiq, and O. Tsioulou, "Combined impact of carbonation and crack width on the chloride penetration and corrosion resistance of concrete structures", Cem. Concr. Compos. 2020 (115), 103819. doi: https://doi.org/10.1016/j.cemconcomp.2020.103819.

[49] W. Wightman, F. Jalinoos, P. Sirles, and K. Hanna, "Application of Geophysical Methods to Highway Related Problems", Blackhawk GeoSciences, a Division of Blackhawk GeoServices. Contract Number:

DTFH68–02-P-00083. Sponsored by Federal Highway Administration Central Federal Lands Highway Div. 555 Zang Street Lakewood, Co 80228, 2003. url: http://www.cflhd.gov/geotechnical

[50] M. H. Z. Abidin, D. C. Wijeyesekera, R. Saad, and F. Ahmad, "The influence of soil moisture content and grain size characteristics on its field electrical resistivity", Elect J Geotech Eng 2013, 18/D: 699-705.

[51] H. Rattez, Y. Shi, A. Sac-Morane, et al. "Effect of grain size distribution on the shear band thickness evolution in sand", Géotechnique 2022, 72:350–363. doi: https://doi.org/10.1680/jgeot.20.P.120

[52] J. Huang, N. Liu, Z. Ma, L. Lu, and K. Dang, "The construction stability of large section tunnel considering the deterioration of clay mechanical properties", Front. Mater. 10:1135276, 2023. doi: https://doi.org/10.3389/fmats.2023.1135276

[53] Federal Ministry of Works and Housing (FMWH), "General Specifications for Roads and Bridges", Volume II.145-284. Federal Highway Department: Lagos, Nigeria, 1997.

[54] S. Ullmann, S. Schmidt, and I. Herle, "Triaxial Compression of Sand-Fines Mixtures at Low Confining Pressures", Geotech Geol Eng (2025) 43:267, 13pp. doi: https://doi.org/10.1007/s10706-025-03251-7

[55] T. Karademir, "Comparison of soil improvement techniques on the development of efficient consolidation response" Turkish Journal of Engineering, 8 (4), 619-639, 2024.

[56] T. V. Tran, D. Alkema, and R. Hack, "Weathering and deterioration of geotechnical properties in time of groundmasses in a tropical climate", Eng. Geol. 260 (2019) 105221, doi: https://doi.org/10.1016/j.enggeo.2019.105221

[57] M. Zoorabadi, I. Canbulat, and M. Ruest, "Probabilistic Slope Stability Analysis as a Tool to Optimise a Geotechnical Site Investigation Program", 2016, pp. 485–491, doi: https://doi.org/10.36487/acg_rep/1604_31_zoorabadi.

[58] C. K. Gbetoglo, P. P. Sarada, D. O. Afolayan, R. R. Amulya, T. S. Tido, A. L. Raoul, A. Babatunde, and P. O. Azikiwe, "Geotechnical and geological investigation of slope stability of a section of road cut debris-slopes along NH-7, Uttarakhand, India" Results in Engineering 10 (2021) 100227, 13pp.

[59] N. Cardozo, and R. W. Allmendinger, Spherical projections with OSXStereonet: Computers & Geosciences, 2013, v. 51, p. 193 – 205, doi: https://doi.org/10.1016/j.cageo.2012.07.021.

[60] R. W. Allmendinger, N. Cardozo, and D. Fisher, "Structural geology algorithms: Vectors and tensors in structural geology": Cambridge University Press (book published in early 2012).

[61] W. Du, B. M. Lehane, J. P. Doherty, and Z. Wang, Z. "Numerical Analysis of Triaxial Tests for Interpreting Sample Stiffness with Existing Measurement Systems", Geotech Geol Eng (2025) 43:280, 14pp. doi: https://doi.org/10.1007/s10706-025-03261-5

[62] G. C. Komadja, S. P. Pradhan, A. R. Roul, B. Adebayo, J. B. Habinshuti, L. A. Glodji, and A. P. Onwualu, "Assessment of stability of a Himalayan road cut slope with varying degrees of weathering: a finite-element-model-based approach", Heliyon 6 (2020), doi: https://doi.org/10.1016/j.heliyon.2020.e05297

[63] Ö. L. Ertugrul, and B. B. Zahin, "A parametric study on the dynamic lateral earth forces on retaining walls according to European and Turkish Building Earthquake Codes", Turkish Journal of Engineering, 7(3), 196-207, 2023.

[64] M. C. Acar, and A. Kekül, "Comparative analysis of an anchored retaining wall system in a deep foundation excavation: A case study of Sivas Cultural Center Building in Türkiye", Turkish Journal of Engineering, 2023, 7(3), 227-235.

[65] Ö. Çimen, and H. İ. Günaydın, "Assessment of engineering geology and grouting applications in Yalnızardıç Dam Site (Antalya, Türkiye)", Turkish Journal of Engineering, 2024, 8 (1), 20-30

[66] A. A. Firoozi, C. G. Olgun, A. A. Firoozi, and M. S. Baghini, "Fundamentals of soil stabilization", International journal of Geo-Engineering (2017) 8:26. doi: https://doi.org/10.1186/s40703-017-0064-9